JOURNAL OF MATERIALS SCIENCE 14 (1979) 2128–2138

Correlations of the craze profile in PMMA with Dugdale's plastic zone profile

S. J. ISRAEL, E. L. THOMAS,* W. W. GERBERICH
Department of Chemical Engineering, University of Minnesota, Minneapolis, Minnesota 55455, USA

The craze opening profile in PMMA has been determined as a function of stress intensity using interference optics and a special wedge loading device. An attempt was made to correlate the craze profile with the corresponding parameters (crack opening displacement and plastic zone length) predicted by the Dugdale model. Over the mid-range of stress intensities (K_I = 0.4 to 1.0 MPa $m^{1/2}$), samples which were annealed after precracking were found to exhibit a profile similar in shape but smaller than that predicted by the Dugdale model. The lower limit of this range marks the critical stress intensity for crazing in PMMA. Both the craze length and the opening at the craze–crack interface increase with increasing stress intensity and, due to strain-hardening of the craze material, reach maximum values of about 40 μm and 3 μm respectively at K_I = 1.0 MPa $m^{1/2}$. Experimental uncertainties cannot account for the profile difference and it is therefore concluded that the Dugdale model is not fully adequate to describe craze geometries in PMMA. The discrepency between the Dugdale model and the experimental data is suggested to be due to either fibril strain-hardening and/or the formation of a plane strain plastic zone ahead of the craze.

1. Introduction

Under tensile stress and/or exposure to various organic solvents glassy amorphous polymers develop what appear to be fine cracks. These structures, called crazes are not cracks in the true sense as they are filled with a cavitated network of highly drawn polymer. The formation of crazes disrupts the mechanical integrity of the matrix. Crazes are generally considered to be directly involved with the processes of crack initiation and propagation and, ultimately, it is craze breakdown which leads to material failure. In spite of these shortcomings crazes are not always detrimental. Crazes do serve a useful purpose from a design standpoint in that large amounts of energy are required in the plastic deformation process necessary for their formation. It is this absorption of energy that greatly enhances the fracture toughness of many engineering plastics.

1.1. Craze profile

When viewed with an optical microscope using incident light, the craze–crack combination is found to exhibit a set of interference fringes. Using interference optics to analyse these fringe patterns one is able to determine the craze–crack opening profile (i.e. the craze or crack opening as a function of distance from the craze tip). The purpose of this investigation was to correlate the craze shape with the plastic zone shape described by the Dugdale model [1]. Specifically, the corrected opening at the craze–crack interface ($\delta - \delta_0$) determined by optical interferometry was correlated with the crack opening displacement (COD), the measured craze length (l_c) was compared with the plastic zone length (R_p) and, the overall profile of the craze ($\delta_t - \delta_0$) was compared with that of the plastic zone (δ).

*Present Address: Polymer Science and Engineering Department, University of Massachusetts, Amherst, Massachusetts 01003, USA

 0022–2461/79/092128–11 $03.10/0

To evaluate R_p and COD from the Dugdale model it is necessary to determine the stress intensity K_I at the crack tip. In previous investigations of this type [2–6], stress intensities corresponding to a given fringe pattern were never actually measured. In two such cases [3, 5], these values were obtained by equating the measured craze length and opening at the craze–crack interface with the corresponding Dugdale parameters (R_p, COD). A yield stress and stress intensity were then back-calculated from the equations describing these parameters. This investigation was, therefore, undertaken in an effort to develop a technique where both the optical interferometry and the stress intensity determination could be performed simultaneously on a single sample. For these measurements a special wedge loading device was constructed which mounts directly on the stage of an optical microscope. Using fracture mechanics, the stress intensity at the crack tip was determined from the measured crack length and forward displacement of the loading wedge.

1.2. Interference microscopy

In 1966, Kambour [7] reported that when the craze–crack combination was viewed with an optical microscope using normal incident light, two distinct sets of interference fringes are seen (see Fig. 1). Subsequent investigation on the origin of these fringes indicates that the larger set of interference fringes, which show a decrease in spacing in the direction of crack propagation, are a result of the crack itself. The more closely spaced set, which shows an increase in spacing in the direction of crack propagation, are a result of a craze which preceeds the crack.

Kambour analysed these fringe patterns using interference optics and was able to determine a craze–crack profile. A number of studies involving the use of the fringe patterns have since been completed. More recently, investigations coupling the profile data obtained from interferometry with models and relations from fracture mechanics have been published [2–6]. In each of these publications, the craze opening profile as determined by optical interferometry was correlated with the plastic zone as described by the Dugdale model.

The observed fringe pattern is a result of the recombination of two beams, one of which is a reflection from the upper surface of the craze and the other from the lower surface (see Fig. 2). The alternating black and white fringe pattern is a result

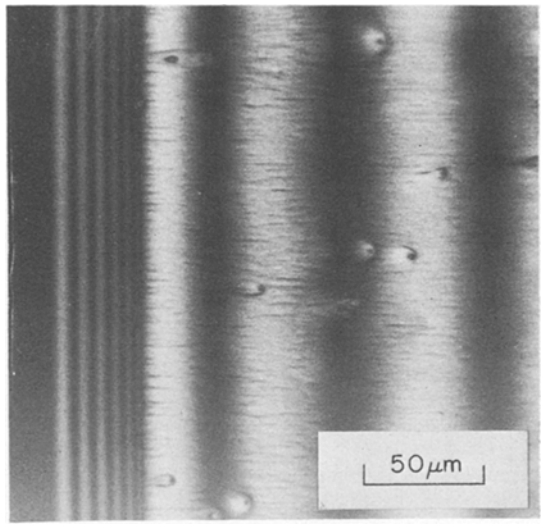

Figure 1 Interference micrograph of craze crack tip showing the two sets of interference fringes.

of the increasing craze thickness, δ, as it opens toward the crack region.

Analysing the fringe pattern using interference optics, an expression for the craze thickness as a function of the wavelength of incident light (λ_v) and the index of refraction of the craze (n_c) is obtained:

$$\text{for bright fringes} \quad \delta = \frac{(m + 1/2)\lambda_v}{2n_c} \qquad (1a)$$

$$m = 0, 1, 2 \ldots,$$

$$\text{for dark fringes} \quad \delta = \frac{m\lambda_v}{2n_c} \qquad (1b)$$

$$m = 1, 2, 3 \ldots.$$

Here, λ_v is determined by the monochromatic filter used in the incident light source. The only unknown is, therefore, the craze refractive index, n_c.

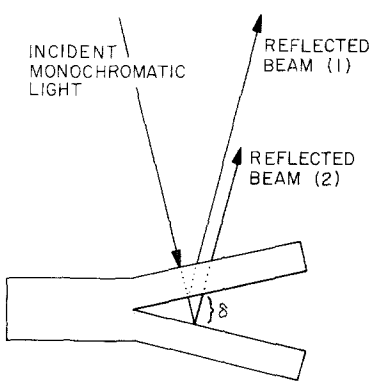

Figure 2 Schematic drawing of the specimen (beam deflection exaggerated) showing the reflection of incident light from the upper and lower surfaces of the craze and crack.

1.3. The Dugdale model

In 1960, Dugdale [1] proposed a model to predict the shape of the plastic zone existing at the crack tip in an elastic–plastic material. His analysis considered a central slit in a thin sheet of material with an applied tensile stress σ normal to the slit (Fig. 3).

Rice [8] applied Westergaard's stress functions to the Dugdale model and found that in plane stress the length of the plastic zone can be related to the stress intensity and yield stress by:

$$R_p = \frac{\pi K_I^2}{8\sigma_{ys}^2}. \tag{2}$$

Moreover, the corresponding seperation distance δ in the plastic zone along $x_2 = 0$ is*

$$\delta = \frac{8\sigma_{ys}R_p}{\pi E^*}\left[\xi - \frac{x_1 - a}{2R_p}\log\left(\frac{1+\xi}{1-\xi}\right)\right], \tag{3}$$

where

$$\xi = \left(1 - \frac{x_1 - a}{R_p}\right)^{1/2}$$

and $$E^* = \begin{cases} E \text{ (plane stress)} \\ E/(1-\nu^2) \text{ (plane strain).} \end{cases}$$

The crack opening displacement (COD) is the value of the separation distance at the crack tip $(x_1 - a = 0)$ (Fig. 4), therefore

$$\text{COD} = \frac{8\sigma_{ys}R_p}{\pi E^*} = \frac{K_I^2}{\sigma_{ys}E^*}. \tag{4}$$

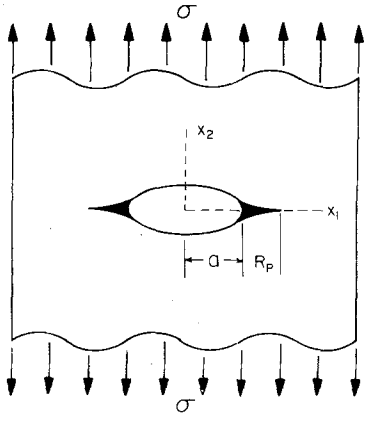

Figure 3 Diagram of the system modelled by Dugdale.

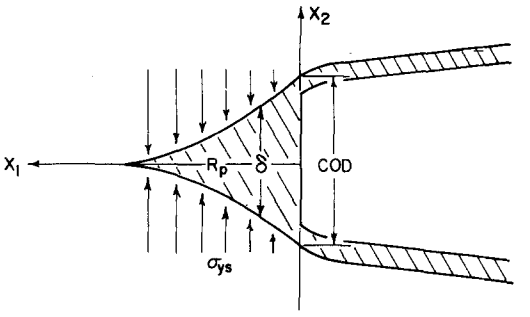

Figure 4 Development of the plastic zone as modelled by Dugdale.

The basic assumptions have been reviewed and the model applied to crazing in glassy polymers [2–6].

2. Experimental methods

As mentioned above, to properly make the correlation between the parameters describing the craze profile and the plastic zone profile, it would be desirable to have a system where both the optical interferometry and the stress intensity determination could be performed simultaneously on a single sample.

Under the constraints of the microscope stage and working distance of the objective lens it was determined that a wedge-loaded double cantilever beam (DCB) specimen would be the preferred design (see Fig. 5). With consideration of the specimen geometry, the loading device was designed to meet the following requirements:

(1) to mount on the microscope stage and allow sample translation,

(2) to keep the craze–crack plane in a fixed position with respect to the objective image plane as the specimen is loaded,

(3) to permit determination of the stress intensity by measuring the forward displacement of the wedge.

2.1. Specimen preparation

Rohm and Haas general purpose (grade G) 0.635 cm (0.25 in.) thick plexiglass sheet was used in this investigation. The molecular weight of this material was measured by gel permeation chromatography and is $\bar{M}_n = 240\,000$, $\bar{M}_w = 940\,000$ yielding $\bar{M}_w/\bar{M}_n$ of 3.9 [10]. The yield strength in tension σ_{ys}, and modulus, E, used in calculations were

*The exact expression for the displacement profile, as given by Goodier and Field [9] differs from Equation 3 by 0.53%.

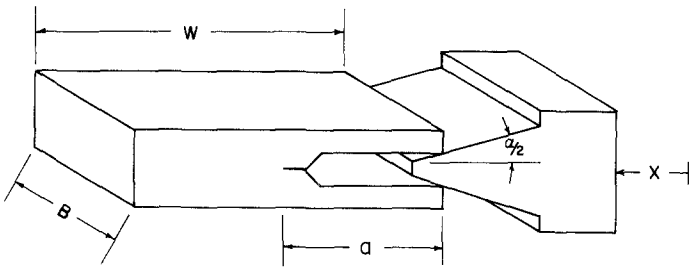

Figure 5 Diagram of the wedge-loading geometry; $W = 5.08$ cm, $B = 2.54$ cm, $a \approx 1.8$ cm, $a/2 = 0.165$ rad.

taken as 7.23×10^7 and 3.1×10^9 Pa, respectively [3, 10]. These properties show only a slight decrease with annealing. Birefringence studies on the as-received material indicated no significant orientation.

The samples were cut with a band saw and milled to size as shown in Fig. 5. Using a small machinists' vise, a razor blade was then slowly driven into the tip of the machined notch to produce a crack preceeded by a craze. Low crack velocities were necessary to maintain control over the length of the crack and to assure that the craze–crack plane lies parallel to the top and bottom surfaces of the specimen.

2.2. Craze–crack opening displacement as determined by Interference fringes

The loading device was mounted on the stage of a Wild M-20 optical microscope. The interference fringes were observed at normal incidence using monochromatic (green, 5460 Å) light. A 35 mm camera mounted directly on the microscope was used to record the fringe patterns.

Lauterwasser and Kramer [11] have proposed that a "primordial craze thickness", δ_0, must be subtracted from the measured craze thickness, δ, to obtain the true displacement in the craze consistent with the displacements of two crack surfaces described in the Dugdale model. This primordial zone is the thickness of polymer which fibrillates to form the craze. Assuming that the volume of polymer remains unchanged during craze formation, the true craze displacement is related to the volume fraction of fibrils within the craze (v_f) as [11]

$$\delta - \delta_0 = \delta(1 - v_f). \tag{5}$$

Kramer [12] has shown that δ_0 depends on the mechanism of craze thickening. For craze thickening by fibril creep as occurs for solvent crazing, δ_0 is essentially constant along the craze, leading to a positionally dependent polymer volume fraction and hence a positionally dependent craze index of refraction. For thickening by fibril drawing as occurs for air crazing, δ_0 increases along the craze, and the index of refraction along the craze is essentially constant. The refractive index of the craze based on measuring the critical angle for reflection of light from fracture surface is reported as 1.32 [7]. Due to relaxation this value is larger than the true index of refraction [13]. Recent transmission electron microscopy experiments [11] for loaded air crazes of several glassy polymers give values of v_F in the range of 0.15 to 0.35. For loaded air crazes in PMMA we have therefore estimated $n_c \simeq 1.10$ (e.g. $v_F = 0.20$). The craze displacement profiles ($\delta - \delta_0$) obtained by optical interferometry were then compared to the plastic zone profiles described by the Dugdale model, i.e. Equation 3.*

Two correlations can be made using the profiles obtained by optical interferometry with those described by Equation 3.

(a) the basis of equivalent plastic zone/craze length, the optically measured craze length is substituted directly for R_p in Equation 3,

(b) the basis of equivalent stress intensity; a plastic zone length R_p used in Equation 3 is determined from the stress intensity obtained from the wedge device using Equation 2.

2.3. Stress intensity determination

Consider a sample being loaded by a wedging force such as that depicted in Fig. 5. For an incremental crack advance under constant load the corresponding strain energy release rate G for a linear elastic material is given by the Irwin–Kies relation [14].

$$G = \frac{P^2}{2BW}\frac{\partial C}{\partial(a/W)}. \tag{6}$$

*Although Equations 2 to 4 were developed for a double-ended crack in an infinite body, they should also be applicable near the tip of the crack ($R_p \ll a$) for the DCB specimen.

Here, P is the applied load, $\partial C/\partial(a/W)$ the change in compliance with incremental increase in crack length, and B and W are the sample thickness and length, respectively. The state of stress at the crack tip is determined by comparing the sample thickness ($B = 2.54$ cm) with the anticipated plastic zone size ($R_p \simeq 40\,\mu$m). Considering the sample thickness is 500 times greater than the plastic zone, it is safe to assume that the loaded sample experiences purely plane strain conditions. The strain energy release rate for plane strain is given by

$$G = \frac{K_I^2}{E}(1-\nu^2), \tag{7}$$

where E is the tensile modulus and ν is Poisson's ratio.

Combining Equations 6 and 7 yields an expression for the stress intensity as a function of the applied load and the derivative of the compliance with respect to crack length, giving

$$K_I = \left\{\frac{P^2E}{2BW(1-\nu^2)}\frac{\partial C}{\partial(a/W)}\right\}^{1/2}. \tag{8}$$

Here, the applied load P cannot be measured directly with the loading device; however, an expression for P can be derived from the geometry of the wedge and the definition of compliance. Consider the situation as depicted in Fig. 5. The wedge has been driven forward to the point where it just starts to exert a load on the sample. This position of the wedge, x_0, is determined from the micrometer. As the wedge is driven forward loading the sample, the deflection (ψ) of the beams of the sample is given by

$$\psi = 2(x-x_0)\tan\alpha/2 \tag{9}$$

where α is the total included angle of the wedge and x is the forward position of the wedge.

Combining this equation with the defining relation for compliance $C = \psi/P$, the desired expression for the applied load is

$$P = \frac{2(x-x_0)\tan\alpha/2}{C}. \tag{10}$$

Substituting Equation 10 into Equation 8 yields an expression for stress intensity with all parameters but the compliance and its derivatives known

$$K_I = (x-x_0)\left\{\frac{2E\tan^2(\alpha/2)}{C^2BW(1-\nu^2)}\frac{\alpha C}{\partial(a/W)}\right\}^{1/2}, \tag{11A}$$

or simply

$$K_I = (x-x_0)f(a/W). \tag{11b}$$

A function expressing the compliance in terms of crack length was developed using the following technique. Eight samples were machined with crack to specimen length ratios (a/W) varying in increments of 0.127 cm (0.05 in.) from 0.635 to 1.524 cm (0.25 to 0.60 in.). Steel tabs were bonded to each specimen and the specimens were then mounted in an Instron tensile testing machine equipped with a 44.96 N (200 lb) load cell and set at a cross-head speed of 0.051 cm min^{-1} (0.02 in. min^{-1}). Here, load–deflection data for small strains were obtained and the compliance of each sample was computed from the slope of the load–deflection output. With the aid of a computer, a polynomial regression was performed on the eight data points (C versus a/W), giving

$$\begin{aligned} C(a/W) = {} & -0.0356 + 0.4652\,(a/W) \\ & - 2.349\,(a/W)^2 + 5.936\,(a/W)^3 \\ & - 7.196\,(a/W)^4 + 3.477\,(a/W)^5. \end{aligned} \tag{12}$$

This function, along with the experimentally determined points, is graphically represented in Fig. 6. Finally, a differentiation with respect to a/W yields the fourth order polynomial needed to completely define the function $f(a/W)$.

$$\begin{aligned} \frac{\partial C}{\partial(a/W)} = {} & \\ & 0.465 - 4.718\,(a/W) + 17.808\,(a/W)^2 \\ & - 28.784\,(a/W)^3 + 17.385\,(a/W)^4. \end{aligned} \tag{13}$$

The stress intensity can now be calculated using Equations 11 to 13 with the measured forward travel of the wedge and the crack length.

To determine whether the values of K_I obtained from Equation 11 under wedge loading were reasonable, other fracture mechanics solutions for the DCB specimen [15–19] were evaluated using one experimental data point. The results of this comparison (see Table I) indicate that the method of determining K_I in this investigation yields a value midway in the range. The span in the calculated values of K_I is due to various simplifying assumptions necessary in applying the rigorous fracture mechanics solutions to the DCB geometry.

TABLE I Comparison of K_I values at crack initiation calculated by different methods for the DCB specimen

Reference	K_I (MPa m$^{1/2}$)
Kanninen [15]	0.58
Paris and Sih [16]	1.40
Robertson [17]	1.59
This study	1.67
Tada *et al.* [18]	1.73
Rice [19]	2.16

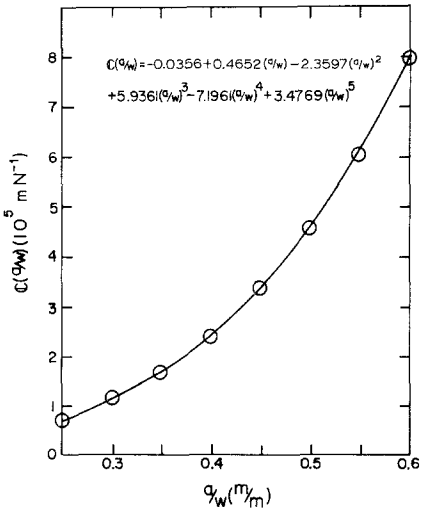

Figure 6 The experimental compliance data ○, and the curve representing the fifth degree polynomial used to describe these data.

Under high loads it is possible that the beams of the specimen undergo plastic deformation yielding a measured stress intensity which is higher than that actually occuring at the crack tip. To check for this deformation the distance between the two beams of the sample was measured with a micrometer before and after loading. No measurable change in this distance was detected. Furthermore, if plastic deformation of the beams were occuring, at high loads the interference fringes near the tip of the crack would not continue to advance with increasing load as was observed.

3. Results and discussion

3.1. $(\delta_t-\delta_0)$–COD, l_c-R_p correlations

Initially, after the razor blade precrack, the specimens were inserted directly into the loading device. Upon analysing the data from these specimens it was found that plots of $\delta_t-\delta_0$ versus K_I and l_c versus K_I were both nearly linear, having initial offsets at zero stress intensity. This anomalous behaviour resulted because of loading the pre-existing craze which occured by precracking. The craze which is formed is composed of highly drawn fibrils under tension. When the razor blade is removed, the sample is allowed to relax thus reducing the tension on the fibrils. Accompanying this relaxation the reduction of fringes within the craze indicates roughly a 50% decrease in the length of the craze fibrils near the craze–crack interface. Therefore, it is likely that the craze fibrils are under compression or have buckled after the razor blade is removed.

Dugdale's model envisions a plastic zone at the crack tip which develops with loading. The plastically deformed material within this zone pulls back elastically exerting a retracting stress on the two surfaces of the crack. This stress is assumed equal to the yield stress of the material (Fig. 4). The situation encountered when reloading the unannealed specimens after the razor blade precrack is quite unlike that modelled by Dugdale. Instead of the material in the plastic zone pulling the surfaces of the crack together, the unannealed specimen has a craze containing compressed or buckled fibrils which effectively push the two surfaces apart (Fig. 7). Here the effective stress on the craze crack region will be a combination of the externally applied stress σ_{app} and the stress produced by the compressed craze material σ_c^*. If the craze fibrils are assumed to behave elastically, the stress produced by the compressed craze material σ_c^* will decrease linearly with craze opening δ. Furthermore, with the absence of retracting forces in the plastic zone or craze, the situation can be treated as the elastic deflection of the double cantilever beam. This deflection is found to behave linearly with the applied load [20]. When the specimen is reloaded with the loading device, the stress necessary for the reopening of the craze depends on the residual compressive stress and

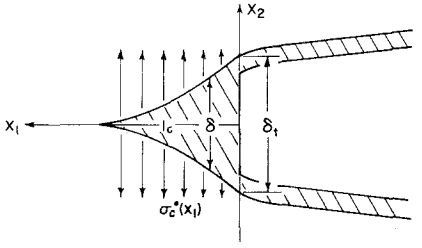

Figure 7 Crack tip situation in unannealed sample where compressed craze fibrils push the craze surfaces apart.

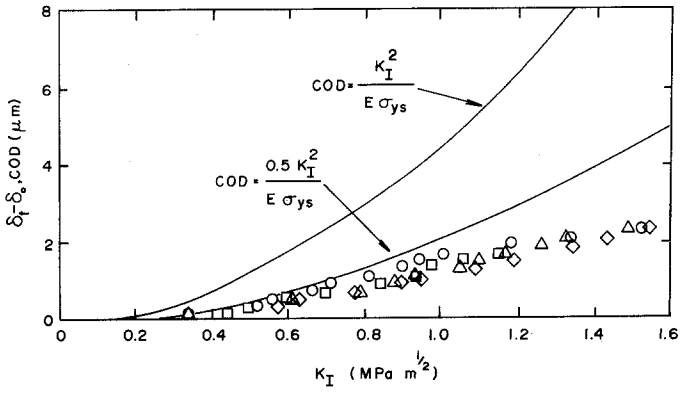

Figure 8 Comparison of $(\delta_t - \delta_0) - K_I$ data for annealed specimens with COD–K_I behaviour predicted by the Dugdale model (upper curve) and a plane strain plastic zone model [25] (lower curve).

since the craze is incompletely healed, a finite δ_t and l_c exists before loading.

To eliminate the effect of the craze formed by precracking, all subsequent specimens were annealed after precracking at temperatures below the glass transition temperature for various lengths of time. This heat-treatment causes the craze to heal thus eliminating the initial COD and relaxing the compressive stresses at the crack tip. When reloading with the wedging device a situation similar to that described by the Dugdale model is encountered.

The results from the annealed specimens shown in Figs. 8 and 9 indicate the following:

(a) below a critical stress intensity (0.3 to 0.4 MPa m$^{1/2}$) optical interferometry indicates that no craze is present. Consequently, both $\delta_t - \delta_0$ and l_c are zero below this critical stress intensity value;

(b) through the mid-range of stress intensities (0.4 to 1.0 MPa m$^{1/2}$) both the displacement $\delta_t - \delta_0$ and craze length l_c are found to lie below but definitely follow the parabolic shape predicted by the Dugdale model;

(c) at high stress intensities (1.0 to $\approx$1.75 (K_{IC}) MPa m$^{1/2}$) $\delta_t - \delta_0$ and l_c reach limiting values of approximately 3 and 40 μm, respectively.

The absence of an experimentally determined crack tip displacement and craze length at low stress intensities can be rationalized using two approaches. First, to obtain the first bright interference fringe the craze thickness must be greater than a quarter of the wavelength of incident light (approximately 0.15 μm thick) at the crack tip. Below this craze thickness, δ_t is undetectable using optical interferometry. A more likely reason for a zero COD at low K_I is that we are observing the critical stress intensity for crazing in PMMA.

Through the mid-range of stress intensities the correlations between $\delta_t - \delta_0$ and COD, and l_c and R_p are found to be quite reasonable. In both cases the experimental data are found to lie parallel to but below that predicted by the Dugdale model. Plots of $\log \delta_t - \delta_0$ versus $\log K_I$ and $\log l_c$ versus $\log K_I$ should each show a slope of 2. Fig. 10 shows these plots. The slopes over the mid-range of stress intensity are found to be 2.05 for $\log \delta_t - \delta_0$ versus $\log K_I$, and 2.05 for $\log l_c$ versus $\log K_I$ indicating quite reasonable agreement with the Dugdale model.

The observation that the experimental data lie below those predicted by the plane stress Dugdale model could be attributed to a number of factors:

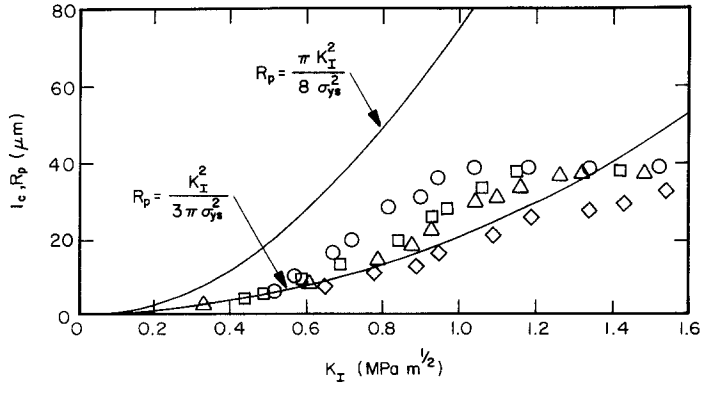

Figure 9 Comparison of l_c–K_I data for annealed specimens with R_p–K_I behaviour predicted by both the Dugdale model (upper curve) and a plane strain zone model (lower curve).

TABLE II

Reference	Craze length l_c (μm)	Opening at craze–crack Interface, δ_t (μm)	State of stress	System
Kambour [7]	25	0.8	Unloaded	Wedge-loaded
	25	1.2	Unloaded	DCB
	25	1.2	Unloaded "Theory"	DCB
	25	1.9	Just prior to failure	DCB
Weidmann and Doll [2]	38	2.9–4.2	Just prior to failure	SEN $T = 20 - 80^\circ$ C
	20–38	1.2–2.9	Just prior to failure	SEN $M_w = 0.11 - 2.2 \times 10^6$
Brown and Ward [3]	24.2	2.95	Unloaded	CTS
	24.2	7.0	Moving craze	CTS
Morgan and Ward [5]	35–28.9	2.2	Just prior to failure	$T = -30 - 45^\circ$ C
Cotterell [6]	25.0	1.8	Unloaded	DCB
This study		$\delta_t - \delta_0$		
	35.5	1.0	Unloaded	Wedge-loaded DCB (not annealed)
	38.5	2.1	Just prior to failure	Wedge-loaded DCB (not annealed)
	0	0	Unloaded	Wedge-loaded DCB (annealed)
	38.8	2.6	Just prior to failure	Wedge-loaded DCB (annealed)

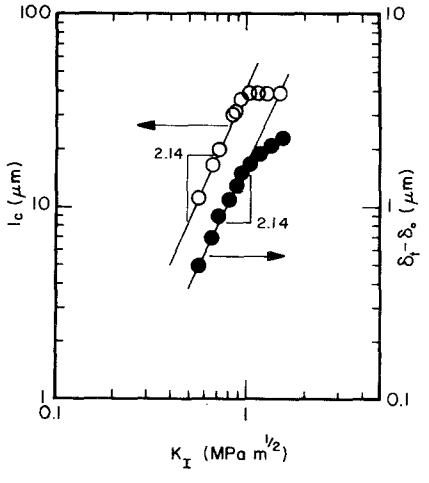

Figure 10 Log $\delta_t - \delta_0$ versus K_I (○) and log l_c versus K_I (●).

(a) the fact that the loading situation is predominantly plane strain while R_p calculations are for plane stress and COD calculations have only been corrected for Poisson effects;

(b) strain-hardening (which would also give rise to the plateau region observed in the $\delta_t - \delta_0$ and l_c versus K_I plots at high stress intensities);

(c) the growth of an initial small plastic zone at the tip of the craze which cannot be detected by optical interferometry.

With increasing stress intensities the craze grows both in length and opening displacement until, at about $K_I = 1.0\,\text{MPa m}^{1/2}$, l_c and $\delta_t - \delta_0$ were found to reach limiting values of approximately 38 and 2.7 μm, respectively. At higher stress intensities material strength resists further craze growth. As can be seen from Table II, l_c and δ_t values rarely exceed 40 and 3 μm, respectively, for PMMA in previous investigations. The smaller values reported are probably a result of relaxation of unloaded crazes which causes the observed craze to decrease both in length and opening displacement. These data strongly suggest that there is a maximum craze lengh and opening at the craze–crack interface for an air craze in PMMA. These limiting values are achieved at 60 to 80% of K_{IC} and do not change with increasing stress intensity until specimen failure occurs at K_{IC}.

3.2. Craze profiles and Dugdale's plastic zone profiles

The craze–crack profiles determined by optical interferometry change with increasing load or stress intensity as shown for the annealed specimen in Fig. 11.

As was discussed above, the craze profile obtained by optical interferometry can be com-

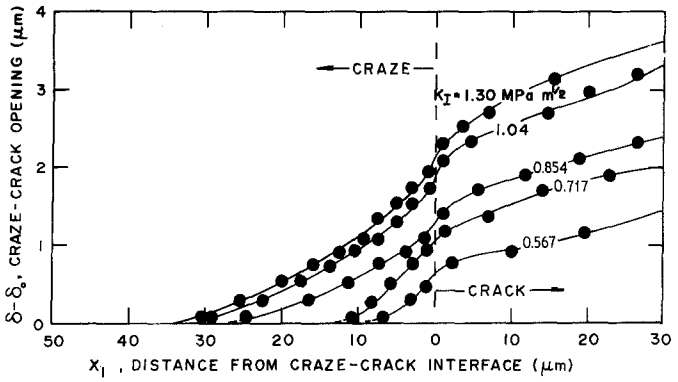

Figure 11 Craze–crack profiles changing with increasing stress intensity.

pared with the plastic zone profiles described by the Dugdale model using two different basis of comparison. Fig. 12a, b and c show the results of both bases of comparison for increasing loads. The results related on the basis of equivalent stress intensity indicate that the profile predicted by the Dugdale model is of the same basic shape but the Dugdale $\delta - K_I$ curve lies above the curve determined by optical interferometry. The profiles determined on the basis of equivalent craze and plastic zone lengths were found to correlate quite well over the mid-range of stress intensities (0.4 to 1.0 MPa m$^{1/2}$).

Recall that the goal of this investigation was to develop a technique where both optical interferometry and the stress intensity determination could be performed simultaneously on the same sample. The measured value of K_I was to be used in the Dugdale expressions for R_p, COD, and $\delta(x_1)$ to determine if the plastic zone described by this model could be used to determine the corresponding craze dimension obtained from optical interferometry. Although the general shape of the plastic zone profile is very close to that of the craze, Fig. 12 indicates a substantial difference in the "magnitude" of the profile curves correlated on the basis of stress intensity. In view of the fact that the measured values of $\delta_t - \delta_0$ and l_c are similar to those reported by other investigators and, that we are confident in the accuracy of the measured stress intensities, it is concluded that the Dugdale plastic zone model is not a fully adequate model to describe are craze geometries in PMMA.

The reason for this inadequacy may be that unlike the well characterized plastic zone deformation described by the Dugdale model, craze growth in PMMA occurs by two simultaneous deformation processes which are further complicated by the effects of strain-hardening of the material [21, 22]. These processes include: the drawing of the craze material – essentially uniaxial tension or plane stress behaviour – and the development of the small plastic zone in front of the craze under a triaxial state of stress – essentially plane strain deformation. Strain-hardening would have the effect of depressing the theoretical COD–K_I and the R_p–K_I curves and could possibly lead to the plateau region at high stress intensities.

If fibril drawing is the controlling process, the parameters described by the plane stress Dugdale

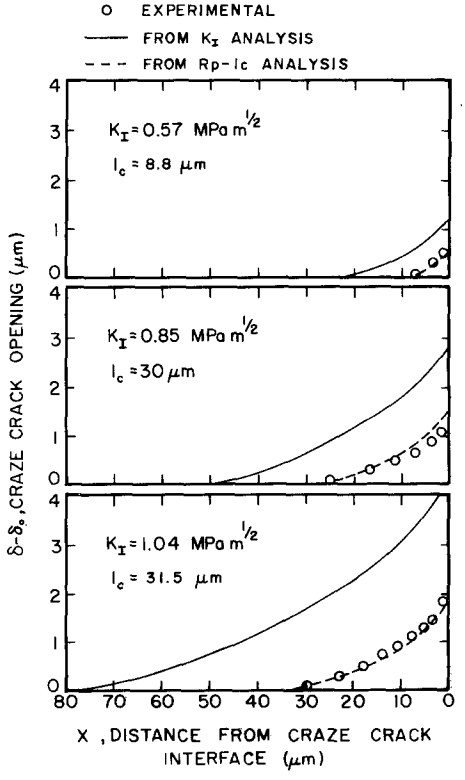

Figure 12 Craze profile correlated with Dugdale plastic zone profile for increasing values of K_I; (O) experimental craze profile, (—) plastic zone profile from equivalent K_I analysis (— — —) plastic zone profile from equivalent l_c–R_p analysis.

model modified to include the effects of strain-hardening should fit the experimental data. Similarly, if plastic zone development were the controlling process, the experimental data should be described by the parameters of a strain-hardening plane strain plastic zone model.

The Dugdale model can be extented to include strain-hardening [23, 24], however, due to its simplicity, the Dugdale model cannot be fully modified for all of the effects of the triaxial state of stress encountered in plane strain loading. To do so, the model would have to include the effects of lateral (Poisson) contractions. But more important is the fact that the primary flow mechanism is constrained yielding and the appropriate flow stress, which includes hydrostatic pressure effects, must be used in the plane strain model (see Appendix).

The most obvious effect of the triaxial state of stress is that the plastic zone geometry changes to a bilobed shape, quite unlike the strip yielding seen in craze formation. All plane strain models describe this type of plastic zone and, therefore, the δ_t–COD correlation is the only one that can realistically be made.

The expression for the COD derived in each of these models [25] is of the form:

$$\text{COD} = \frac{AK_I^2}{\sigma_{ys}E}, \tag{14}$$

where Poisson effects and the change in yield stress due to the triaxial state of stress are included in the numerical coefficient A. For plane strain models that have not been modified for strain-hardening, the COD under plane strain loading conditions is approximately 50% of that described by the Dugdale model (plane stress). The correlation between the experimental data and the unmodified plane strain plastic zone model (for $A = 0.5$) are shown in Fig. 8. Similar correlations for the unmodified plane strain plastic zone length:

$$R_p = \frac{K_I^2}{3\pi\sigma_{ys}^2} \tag{15}$$

are shown in Fig. 9.

Craze growth may be controlled by a combination of fibril drawing and plastic zone formation. Therefore, the experimental data should lie between the extremes of strictly plane stress and plane strain behaviour both modified for the effects of strain-hardening.

The results show (Fig. 8, 9) that over the entire range of stress intensities the experimental data lie mostly on, or below, the curve described by the unmodified plane strain model. However, the extent of the depression of the curves due to strain-hardening is not known. Therefore, a choice between fibril drawing or constrained yielding ahead of the craze as the process controlling air craze growth in PMMA cannot be made, at present.

4. Conclusions

Correlations have been made in an effort to determine if the plastic zone shape described by the Dugdale model can be used to predict the craze profile in PMMA. The following conclusions are drawn.

(1) Through the mid-range of stress intensities ($K_I = 0.4$ to $1.0\,\text{MPa}\,\text{m}^{1/2}$) the samples which were annealed after the razor blade precrack were found to exhibit a behaviour similar to that predicted by the Dugdale model.

(2) There is a critical stress intensity for craze formation at 0.3 to $0.4\,\text{MPa}\,\text{m}^{1/2}$.

(3) At stress intensities above $1.0\,\text{MPa}\,\text{m}^{1/2}$ the craze length and opening at the craze–crack interface were found to reach maximum values of about 40 and 3 μm, respectively. This plateau is suggested to be due to strain-hardening of the material.

(4) The profile described for a plastic zone with a length equivalent to that of the craze gave excellent agreement.

(5) For profiles based on the measured stress intensity the general shape of the plastic zone profile was very close to that of the craze but the calculated plastic zone profile was found to be much larger.

(6) The discrepency between the existing model and the experimental data is suggested to be due to either strain-hardening or to the formation of a plane strain plastic zone ahead of the craze.

Appendix

For polymers there is a strong dependence of yield stress on hydrostatic pressure. Therefore, in the interpretation of plastic zones, plastic strain distributions or plastic energy dissipation at crack tips, the theories developed for metals must be modified. For example, both Bauwens [26] and Sternstein *et al.* [27] have derived a modified von Mises yield criterion where the shear yield stress is given by

$$\tau_m = \tau_m^0 + \mu_m P \tag{A 1}$$

Here, μ_m is a constant, P is $-(tr\sigma)/3$ and τ_m^0 is the yield stress in pure shear. It can be shown that when the stress field about a crack is substituted into the von Mises yield criterion, a different size and shape of plastic zone is obtained. Using this inverse method, the elastic–plastic boundary of a plane strain mode I crack is given by

$$6\left\{\frac{\sigma_{ys}}{\sqrt{3}} - \mu_m\left[\frac{(1+\nu)}{3}\frac{2K_I}{\sqrt{(2\pi r)}}\cos\left(\frac{\theta}{2}\right)\right]\right\}^2 = \frac{K_I^2}{\pi r}\cos^2\left(\frac{\theta}{2}\right)\left[1 + 3\sin^2\left(\frac{\theta}{2}\right) - 4\nu(1-\nu)\right], \quad (A\,2)$$

where ν and θ are polar co-ordinates about the crack tip. For PMMA, calculation shows that for the plane strain mode I loading, the average plastic zone length along all possible rays would be about 1.6 times as long as that predicted from a yield criterion, which ignores the hydrostatic pressure. Along the line of the crack, $\theta = 0$, this ratio is 3.3. Similarly, for plane stress mode I loading these ratios were found to be 1.3 and 1.4, respectively.

Acknowledgements

The support of a Xerox Fellowship (for SJI) is gratefully acknowledged. We also appreciate helpful discussions with Professor E. J. Kramer.

References

1. D. S. DUGDALE, *Mech. Phys. Solids* 8 (1960) 100.
2. G. W. WEIDMANN and W. DOLL, Abstracts from Third International Conference on Deformation, Yield and Fracture of Polymers (1976).
3. H. R. BROWN and I. M. WARD, *Polymer* **14** (1973) 469.
4. N. J. MILLS and N. WALKER, *ibid* **17** (1976) 335.
5. G. P. MORGAN and I. M. WARD, *ibid* **18** (1977) 87.
6. B. COTTERELL, *Int. J. Fract. Mech.* **4** (1968) 209.
7. R. P. KAMBOUR, *J. Polymer Sci. A-2* **4** (1976) 349.
8. J. R. RICE, Proceedings of the First International Conference on Fracture (Sendai), Vol. 1 (Japanese Society for Strength and Fracture of Materials, Tokyo, 1966) 283.
9. J. N. GOODIER and F. A. FIELD, "Fracture in Solids", edited by D. C. Drucker and J. J. Gilman (Interscience, New York, 1963).
10. Plexiglass G. Product Literature, Rohm and Haas Company, Philadelphia, PA.
11. B. D. LAUTERWASSER and E. J. KRAMER, MSC Report #3076, Cornell University (1978).
12. E. J. KRAMER, "Developments in Polymer Fracture", edited by E. H. Andrews (Applied Sciences, London, 1979).
13. M. J. DOYLE, *J. Mater. Sci.* 8 (1973) 1185.
14. G. R. IRWIN and J. A. KIES, *Welding J. Res. Suppl.* **33** (1954) 1935.
15. M. F. KANNINEN, *Int. J. Fract.* **9** (1973) 83.
16. P. PARIS and G. SIH, in "Frature Toughness Testing and Its Applications", ASTM STP 381, Philadelphia (1965).
17. R. E. ROBERTSON, *J. Adhesion* 7 (1975) 121.
18. H. TADA, P. PARIS and G. IRWIN, "The Stress Analysis of Cracks Handbook" (Del Research Corporation, Hellertown, Penn, 1973).
19. J. R. RICE, in "Fracture", edited by H. Leibowitz (Academic Press, New York, 1968).
20. C. O. HARRIS, "Introduction to Stress Analysis" (MacMillan, New York, 1959).
21. O. K. SPURR Jr. and W. D. NEIGISCH, *J. Appl. Polymer Sci.* **6** (1962) 585.
22. R. D. KAMBOUR and R. W. KOPP, *J. Polymer Sci. A-2* 7 (1969) 183.
23. J. C. NEWMAN Jr., *Eng. Fract. Mech.* **1** (1963) 137.
24. G. T. HAHN and A. R. ROSENFIELD, *Acta Met.* **13** (1965) 293.
25. R. W. HERTZBERG, "Deformation and Fracture Mechanics of Engineering Materials" (Wiley, New York, 1976).
26. J. C. BAUWENS, *J. Polymer Sci. A-2* **5** (1967) 1145.
27. S. S. STERNSTEIN, L. ONGCHIN and A. SILVERMAN, *Appl. Polymer Symp.* 7 (1969) 175.

Received 8 March and accepted 23 November 1978.